POLITECNICO
MILANO 1863

SCUOLA DI INGEGNERIA INDUSTRIALE
E DELL'INFORMAZIONE

Executive Summary of the Thesis

Formulation and numerical solution of quantum batteries optimal control problems

Laurea Magistrale in High Performance Computing Engineering - Ingegneria del Calcolo ad Alte Prestazioni

Author: Emanuele Broggini

Advisor: Prof. Gabriele Ciaramella

Co-advisors: Dr.Kieran Hymas,Dr.James Quach (The Commonwealth Scientific and Industrial Research Organisation)

Academic year: 2023-2024

1. Introduction

Quantum batteries offer advanced energy storage by utilizing quantum properties like entanglement and coherence. Research focuses on optimizing interactions among components such as molecules and photons to enhance performance. Potential benefits include higher energy capacity, faster charging, and sustainability. Recent work shows superabsorption [3] can boost charging power through collective effects. This thesis explores control strategies for improving quantum battery design and charging efficiency.

2. The Physical Model: Quantum Battery's Hamiltonian and Lindblad Master Equation

This thesis investigates a quantum battery system composed of molecules coupled to a cavity photon field, aiming to optimize energy transfer efficiency through external control and charge separation via fermionic leads. More specifically, the reduced system, denoted by $\mathcal{S}$, comprises the N_p molecules strongly coupled to the photon field within the cavity. The Hamiltonian of the system describes the interactions between these components. The environment, represented by $\mathcal{B}$, consists of electronic reservoirs (source and drain) that facilitate the exchange of particles and energy with $\mathcal{S}$.
The total Hamiltonian of the system is given by:

$$\begin{aligned}\hat{H} = \hat{H}_{\text{mol}} \otimes \hat{I}_{\text{cav}} + \hat{I}_{\text{mol}} \otimes \hat{H}_{\text{cav}} \\ + \hat{H}_{\text{hop}} \otimes \hat{I}_{\text{cav}} + \hat{H}_{int} + \hat{V}(t),\end{aligned} \tag{1}$$

where $\hat{H}_{\text{mol}}$ is the Hamiltonian of the molecules, $\hat{H}_{\text{cav}}$ is the Hamiltonian of the photon field, $\hat{H}_{\text{hop}}$ is the hopping Hamiltonian, $\hat{H}_{\text{int}}$ is the light-matter interaction, and $\hat{V}(t)$ is the time-dependent driving field. The Hamiltonian is expressed in the rotating frame of the laser, using the rotating wave approximation.
The reduced system $\mathcal{S}$ includes chromophores and the photon field, with Hilbert spaces $\mathcal{H}_{\text{mol}}$ and $\mathcal{H}_{\text{cav}}$. The molecular Hamiltonian $\hat{H}_{\text{mol}}$ encompasses the HOMO and LUMO energy levels, while $\hat{H}_{\text{cav}}$ pertains to the photon field energy in the cavity. The light-matter interaction $\hat{H}_{int}$

is crucial for energy transfer between molecules and photons. The driving field $\hat{V}(t)$ controls the photon population in the cavity, affecting energy transfer via the interaction Hamiltonian $\hat{H}_{int}$. Intermolecular hopping is represented as a coherent term in Lindblad dynamics by the Hamiltonian $\hat{H}_{hop}$. The reduced system's Hilbert space dimension $\mathcal{H}_S$ is $N \times M$, where $N = 4^{N_p}$, indicating complexity with N_p molecules and a finite subspace for the photon cavity allowing M Fock states.

The interplay between coherent evolution and incoherent charge transport processes in the quantum battery is effectively described by the following Lindblad master equation:

$$\dot{\hat{\rho}} = -i[\hat{H}, \hat{\rho}] + \sum_k \gamma_k \cdot \mathcal{L}[\hat{O}_k](\hat{\rho}), \qquad (2)$$

where the sum in Eq. (2) concisely represents the battery's interaction with the charge reservoirs.

The Lindblad equation incorporates both coherent evolution and incoherent processes, with the latter being crucial for describing dissipation and decoherence in open quantum systems like the battery. These incoherent processes, represented by Lindblad superoperators, are responsible for energy relaxation, charge transfer, and loss of quantum coherence due to interaction with the environment.

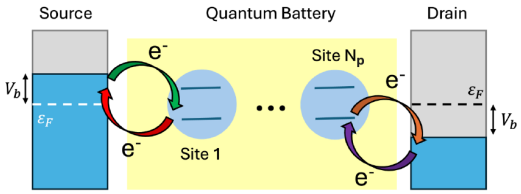

Figure 1: Schematic representation of the quantum battery model, illustrating the coupling between the battery and the electrodes described by the Lindblad equation.

3. Real Formulation of the Lindblad equation

The Lindblad master equation describes the dynamics of open quantum systems but poses computational challenges, particularly for complex systems and quantum optimal control. A more practical formulation is necessary for efficient simulations and analysis. The real matrix formulation enables the use of optimization techniques from control theory, like gradient-based and Newton-type algorithms. As noted in [2]-[1], matrix representation is crucial for managing control constraints, such as radiofrequency pulse limitations in NMR.

3.1. Construction of the basis

To represent the Lindblad equation in matrix form, an orthonormal basis of Hermitian operators has been constructed for the Hilbert space $\mathcal{H}_S$. The basis $\mathcal{B} = \{\hat{B}_{ij}\}$ is obtained by combining, via Kronecker products, orthonormal bases constructed separately for the Hilbert subspaces of molecules ($\mathcal{H}_{\text{mol}}$) and the photon field ($\mathcal{H}_{\text{cav}}$). The basis for $\mathcal{H}_{\text{mol}}$ is generated by Kronecker products of Pauli matrices, while the basis for $\mathcal{H}_{\text{cav}}$ is constructed using orthonormal Hermitian matrices. The total dimension of the basis for $\mathcal{H}_{\text{mol}}$ is $N^2 \times M^2$, where N and M are the dimensions of the two Hilbert subspaces.

3.2. Matrix representation of the density operator

Using the basis for the total Hilbert space, the density operator $\hat{\rho}$ can be represented as a vector of real values $\mathbf{x}$ of dimension $N^2 \times M^2$. To establish this representation, we first define the linear map $V : \mathfrak{her}(N \times M) \to \mathbb{R}^{N^2 \times M^2}$ as

$$V(\hat{\rho}) = \left(\langle \hat{\rho}|\widehat{B}_1\rangle, \langle \hat{\rho}|\widehat{B}_2\rangle, \ldots, \langle \hat{\rho}|\widehat{B}_{N^2\times M^2}\rangle\right)^T$$

where $\langle\cdot|\cdot\rangle$ is the inner product on the space $\mathfrak{her}(N)$, namely $\langle A, B\rangle = \text{Tr}(A^\dagger B)$ for $A, B \in \mathfrak{her}(N)$.

The generalized Bloch vector

$$x = (x_1, x_2, \ldots, x_{N^2\times M^2})^T := V(\hat{\rho})$$

represents the density operator $\hat{\rho}$ in the chosen basis $\mathcal{B}$. A Liouville superoperator $\mathcal{L}_{\hat{H}}$ associated with a Hamiltonian $\hat{H}$ is defined as $\mathcal{L}_{\hat{H}}(\cdot) = -i[\hat{H}, \cdot]$, then we can reformulate the Eq. (2) as

$$\begin{aligned}\dot{\hat{\rho}} = &\mathcal{L}_{\hat{H}_0}(\hat{\rho}) + \mathcal{L}_{\hat{H}_{int}}(\hat{\rho}) \\ &+ \mathcal{L}_{\hat{H}_{hop}}(\hat{\rho}) + \sum_k \gamma_k \cdot \mathcal{L}[\hat{O}_k](\hat{\rho}) \\ &+ \mathcal{L}_{\hat{V}(t)}(\hat{\rho}).\end{aligned}$$

The reformulated equation constructs matrices A and B to convert a time-dependent function into a scalar control parameter and derive the linear differential equation system $\dot{x} =$

$Ax + uBx$. This approach is essential for quantum battery system analysis and control. The total matrix A includes contributions from the free Hamiltonian, light-matter interaction, hopping Hamiltonian, and Lindblad superoperators, defining the quantum battery's dynamics, which are crucial for understanding and control. Matrix B uses scalar products derived from the time-dependent driving field operator to represent the control field's effect on system dynamics. It simplifies the operator by expressing the control field as a scalar variable to reformulate the superoperator. $\eta(t)$ denotes the time-dependent control field, subsequently expressed as a scalar variable $u(t)$ within the matrix formalism.

4. Optimal Control

Optimal control theory finds the best control input to optimize a system's goal by defining its dynamics, state variables, control inputs, objective function, and constraints. This thesis uses optimal control to enhance charging and minimize discharging in a quantum battery. By adjusting the external driving field $\eta(t)$, energy transfer between cavity photons and molecules is regulated, optimizing performance, improving charging efficiency, reducing discharge energy loss, and exploring performance limits.

4.1. Quantum Battery Charging and Discharging

This section formulates the optimal control problem for charging and discharging a quantum battery. The cost functional, representing the mean energy at time T, is defined as $J(x,u) = \pm c^T x(T) + \frac{\nu}{2}\|u\|^2_{L^2(0,T)}$, where $c^T x(T)$ corresponds to $\langle\hat{\rho}(T)|\left(\hat{H}_{mol} + \hat{H}_{hop}\right)\otimes\hat{I}_{cav}\rangle$ and a regularization term penalizes large control inputs. The goal is to find the control input $u(t)$ that minimizes this cost functional, subject to the system's dynamics, to optimize the energy storage or extraction process.

The initial state of the quantum battery, x_0, is crucial for defining the optimization problem. For discharging, x_0 is the highest energy eigenstate of the Hamiltonian molecular subsystem $\left(\hat{H}_{mol} + \hat{H}_{hop}\right) \otimes \hat{I}_{cav}$, representing a fully charged battery. The goal is to minimize the extracted energy. For charging, x_0 is the lowest energy eigenstate, representing the initial state of the quantum battery before any charging has occurred. In this state, the battery is in its resting state, with minimal energy. The goal is to maximize the stored energy by driving the system to higher energy levels.

4.2. Pontryagin Maximum Principle

Pontryagin's Maximum Principle (PMP) is employed to find the optimal control for the quantum battery. The Hamiltonian function, $\mathcal{H}(x,u,p)$, combines the dynamics of the system with the cost functional. It is defined as

$$\mathcal{H} : \mathbb{R}^{N^2\times M^2} \times \mathbb{R} \times \mathbb{R}^{N^2\times M^2} \to \mathbb{R}, \quad \text{s.t.}$$
$$\mathcal{H}(x,u,p) := \langle p, f(x,u)\rangle + \frac{\nu}{2}\|u\|^2_{L^2(0,T)}. \quad (3)$$

The PMP provides necessary conditions for optimality:

- State Equation: $\dot{x}^*(t) = \frac{\partial\mathcal{H}}{\partial p}(x^*(t),u^*(t),p^*(t)) = [A + u^*(t)B]x^*(t)$,
- Adjoint Equation: $\dot{p}^*(t) = -\mathcal{H}_x(x^*(t),u^*(t),p^*(t)) = -(A + u^*(t)B)^T p^*(t)$,
- Terminal Condition: $p^*(T) = c$
- Minimization of Hamiltonian: $\mathcal{H}(x^*,u^*,p^*) \le \mathcal{H}(x^*,v,p^*), \forall v \in \mathbb{R}$.

These conditions lead to the gradient condition $\nabla_u\mathcal{H}(x,u,p) = \nu u + p^T Bx = 0$, which is crucial for implementing the gradient descent algorithm. The initial state, x_0, is chosen based on whether the battery is being charged or discharged.

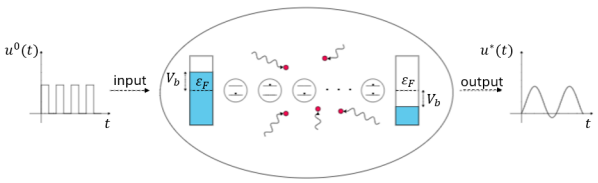

Figure 2: The schematic represents a simplified model of a quantum battery and its control process. The goal is to show how an input control signal $u^0(t)$ influences the state of the battery, leading to a desired output signal $u^*(t)$.

5. Gradient Descent Method

The gradient descent method is employed to optimize control parameters in the quantum bat-

tery system. To maximize charge, the problem is reformulated as a minimization problem: $\min_{x,u} J(x,u) = -c^T x(T) + \frac{\nu}{2}\|u\|^2_{L^2(0,T)}$. The gradient of the reduced cost functional, $\nabla_u \hat{J}(u) = \nu u - \langle Bx, p\rangle$, is used to iteratively update the control input. The state x and adjoint state p are determined by the system's dynamics and final conditions, respectively. This approach allows for efficient optimization of the quantum battery's charging process.

Gradient descent iteratively minimizes a function by moving in the direction of the negative gradient, which points to the steepest descent. It starts with an initial guess and refines it by updating with steps along the negative gradient to minimize costs. The step size is critical for convergence. We use the Armijo line search, a backtracking method, to ensure sufficient decrease of the objective function. Convergence depends on the size of the step and the initial guess. We employ a stopping criterion based on gradient norm tolerance and maximum iterations, ensuring that the algorithm converges to a local minimum.

6. Numerical Experiments and Discussion

This chapter presents the quantum control optimization results for a quantum battery system. To enable a more accurate analysis of the fundamental behavior of the system, we considered the smallest possible system dimensions, namely $N_p = 2$ and $M = 3$. We begin by analyzing the system's structure and spectral properties using graph connectivity. The free dynamics without control serve as a baseline. The focus is on optimizing state transitions through a gradient descent algorithm to minimize cost. We discuss algorithm convergence, optimal control signals, and system response to intermolecular hopping and dissipation, evaluating robustness and the effect of hopping on state connectivity. Lastly, we present the optimized battery charging results and the study's contributions.

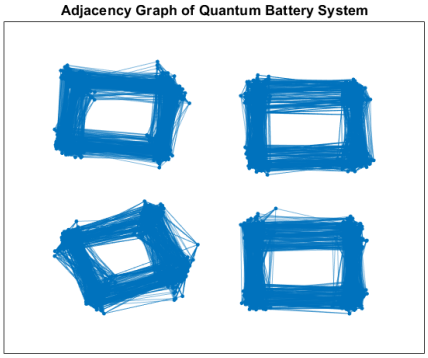

Figure 3: Adjacency graph representing the connectivity between states in the quantum battery system in which the hopping term and the Lindblad superoperators are not included.

6.1. Graph Connectivity Analysis

An analysis of the system connectivity revealed the presence of interconnected state blocks. Notably, the connectivity graph in Fig.4 representing the eigenstates of the Hamiltonian $\hat{H}_0 + \hat{H}_{int}$ shows triangular structures (e.g., 1-2-4, 27-32-37, 12-17-22, 47-48-45) indicating transitions occurring exclusively between photonic states, effectively bypassing interaction with the molecular subsystem. These eigenstates reside within the kernel of the interaction Hamiltonian $\hat{H}_{int}$. Conversely, transitions involving eigenstates outside these triangular structures exhibit an effective charging of the molecular component alongside the photonic component.

Since we are trying to maximize the energy stored in the matter part of the battery, we will not consider transitions between pure photonic states, focusing on state transitions that involve the matter part of the battery.

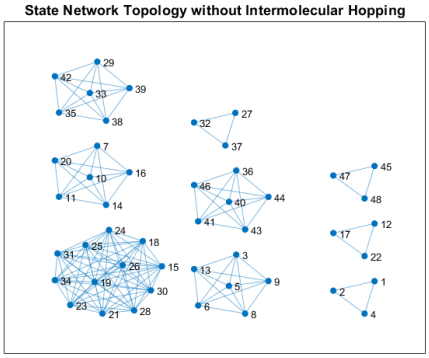

Figure 4: Network topology of the system representing the connectivity between states in the quantum battery system without the hopping term and dissipation.

Optimization can then focus on the core block to reduce computational complexity.

6.2. Spectral Properties of A and Free Evolution of the system

Spectral analysis of the system matrix revealed the natural oscillation frequencies and the existence of steady states. The free evolution of the system shows that some components converge to steady states, while others oscillate. The former are associated with negative real eigenvalues, while the latter are associated with imaginary eigenvalues. The free evolution analysis of the system provided a basis for comparing the effectiveness of optimal control, revealing the presence of decay and oscillation modes.

6.3. Methodology and Optimization Parameters

The quantum battery charging was optimized using the Gradient Descent algorithm with Armijo Line Search. The cost functional J to minimize is given as

$$J(x,u) = -x_d^T x(T) + \frac{\nu}{2}\|u\|^2_{L^2(0,T)}, \qquad (4)$$

, with $x(T)$ as the system's final state, x_d the desired final state, ν the regularization parameter, and u the control signal. Minimizing $J(x,u)$ equates to maximizing the overlap $x_d^T x(T)$ between the final and desired states, transitioning the battery from its initial state x_0 to x_d. The battery's energy at the final time T is computed as $E(T) = c^T x(T)$, using c, a vector from the Hamiltonian $\hat{H}$. Vectors x_0 and x_d derive from eigenstates of the static Hamiltonian. Simulations confirm the effectiveness of the algorithm for transitions from x_0 to x_d. Implemented in MATLAB, the algorithm uses variable iterations and gradient tolerance based on the state transition, with the regularization parameter at $\nu = 10^{-8}$. The final energy $E(T)$ and the cost functional J are evaluated using the mentioned equations.

6.4. System Analysis Without Hopping and Dissipation

The Gradient Descent algorithm's convergence was analyzed under idealized conditions ($t_h = 0$, $\Gamma = 0$). Network topology analysis revealed triangular structures representing pure photonic transitions, which were excluded from further optimization due to their irrelevance to molecular energy storage.

Successful Transitions

(x_0, x_d)	Iter.	$E(T)$	$\hat{J}(u)$	$\|\nabla_u \hat{J}(u)\|_\infty$
(x_1, x_2)	80	-1.33	-1.00	8.7E-5
(x_1, x_4)	80	-2.66	-1.00	2.7E-5
(x_2, x_4)	21	-2.66	-1.00	5.5E-6
(x_{12}, x_{17})	78	-7.79	-1.00	8.5E-6
(x_{12}, x_{22})	80	-9.12	-1.00	2.7E-5
(x_{17}, x_{22})	21	-9.13	-1.00	5.5E-6

Table 1: Selected transitions ($\Gamma = 0$, $t_h = 0$). Maximum of 80 iterations and tolerance set to $1,0 \times 10^{-6}$.

Successful Transitions for $x_0 = 3$

(x_0, x_d)	Iter.	$E(T)$	$\hat{J}$	$\|\nabla_u \hat{J}(u)\|_\infty$
(x_3, x_5)	2000	-2.79	-0.93	6.3E-3
(x_3, x_8)	2000	-2.85	-0.96	4.5E-3
(x_3, x_9)	2000	-3.26	-0.91	3.5E-3

Table 2: Selected transitions ($\Gamma = 0$, $t_h = 0$), starting from the ground state $x_0 = 3$ involving the molecular subsystem. Maximum of 2000 iterations with tolerance set to $1,0 \times 10^{-4}$.

As shown in Tables [1] [2], successful transitions were achieved with convergence demonstrated for both photonic and matter subsystems, specifically for transitions from the ground state $x_0 = 3$ to excited states.
Convergence analysis $x_0 = 3 \to x_d = 8$ shows the cost functional $\hat{J}(u)$ nears -1, indicating op-

timal overlap between final and desired states. A stable energy $E(T)$ confirms successful charging. Complex optimal control $u^*(t)$ means precise, nonperiodic modulation of the driving field is needed for energy transfer. Convergence of $\hat{J}(u)$ to -1 ensures perfect charge, maximizing final state overlap. Stable energy $E(T)$ signifies cost functional minimization, while fluctuating control $u^*(t)$ calls for dynamic photon injection adjustments for efficient storage.

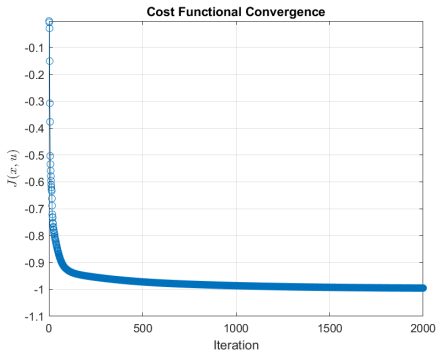

Figure 5: Evolution of $\hat{J}(u)$ over iterations for transition $x_3 \rightarrow x_8$.

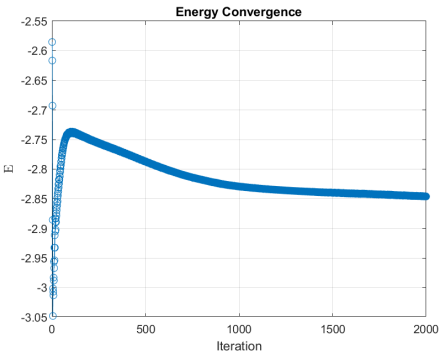

Figure 6: Evolution of energy $E(T)$ over iterations for transition $x_3 \rightarrow x_8$.

6.5. Optimal Control Robustness Analysis

The robustness of pre-computed optimal controls $u^*(t)$ was analyzed against variations in intermolecular hopping (t_h) and dissipation (Γ).

6.5.1 Robustness Against Intermolecular Hopping (t_h)

The cost functional $\hat{J}(u^*)$ remained close to its optimal value for the values of t_h up to approximately 7.5×10^{-2} eV as shown in Fig.8, indicating robustness against small hopping perturbations. However, beyond 10^{-2} eV, a significant degradation in performance was observed.

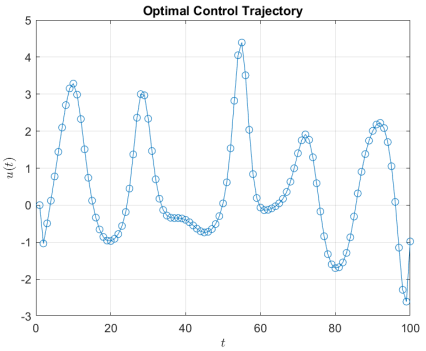

Figure 7: Optimal control $u^*(t)$ for transition $x_3 \rightarrow x_8$.

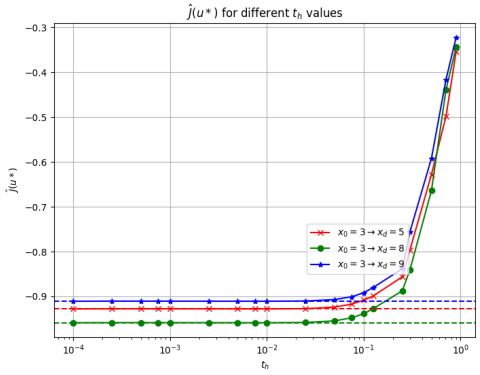

Figure 8: Variation of the cost functional $\hat{J}(u^*)$ as a function of the hopping probability amplitude t_h (eV) for the transitions $x_0 = 3 \rightarrow x_d = 5$, $x_0 = 3 \rightarrow x_d = 8$ and $x_0 = 3 \rightarrow x_d = 9$.

6.5.2 Robustness Against Dissipation (Γ)

Optimal controls were robust against dissipation up to $\Gamma = 10^{-2}$ as shown in Fig.9, beyond which significant performance degradation occurred. This indicates robustness under realistic dissipative conditions.

6.5.3 Combined Impact of Hopping and Dissipation

3D surface plot in Fig. 10 showed a robustness region at low t_h and Γ values. The control was more sensitive to Γ variations than t_h, emphasizing the greater impact of dissipation on performance.

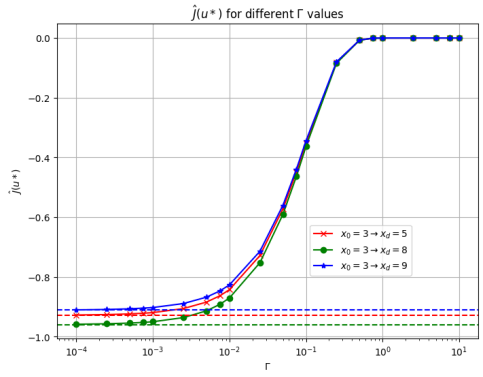

Figure 9: Variation of the cost functional $\hat{J}(u^*)$ as a function of the charge hopping rate Γ (s^{-1}) for the transitions $x_0 = 3 \to x_d = 5$, $x_0 = 3 \to x_d = 8$ and $x_0 = 3 \to x_d = 9$.

These analyses highlight the importance of minimizing both hopping and dissipation in quantum battery charging protocols, as deviations can significantly impact charging efficiency.

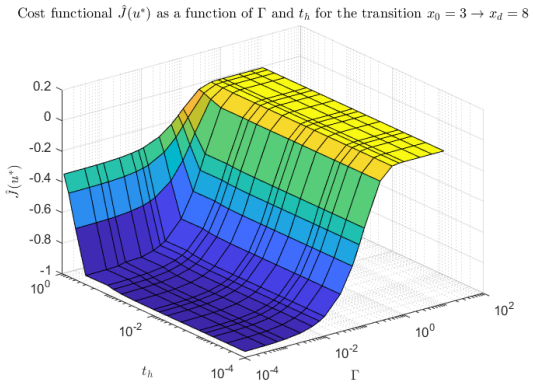

Figure 10: Variation of the cost functional $\hat{J}(u^*)$ as a function of the charge hopping rate Γ (s^{-1}) and of the hopping probability amplitude t_h (eV) for the transition $x_0 = 3 \to x_d = 8$.

6.6. Optimization of Transitions with Hopping and Dissipation

The transition $x_0 = 3 \to x_d = 5$ was optimized considering intermolecular hopping and dissipation, using a specific hopping amplitude $t_h = 1.0 \times 10^{-4}$ and a dissipation rate $\Gamma = 1.0 \times 10^{-3}$. Rapid convergence of the cost functional $\hat{J}$ and the gradient norm $\|\nabla_u \hat{J}(u)\|_\infty$ confirmed the effectiveness of the algorithm. The increased and stabilized energy to the value $E(T) = -2.7$eV indicated that the control field successfully directed the system to the desired state. The optimal control $u^*(t)$ in Fig.11 featured pronounced peaks early and midway, followed by damped oscillations, which required an initial and mid-stage intensity with precise modulation.

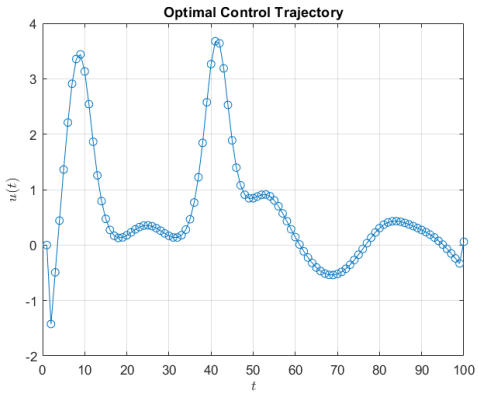

Figure 11: Optimal control $u^*(t)$ for transition $x_3 \to x_5$ with the inclusion of the hopping term and dissipation in the system.

6.7. Optimization of Battery Charge

The quantum battery's overall charge was optimized by maximizing the expectation value of the molecular Hamiltonian as explained in Section 4.1. The complete dynamics of the system, including hopping and dissipation, was considered. The optimization starts from the ground state $x_0 = 3$.

The cost functional $\hat{J}(u)$ converged rapidly, indicating effective maximization of battery charge. The gradient norm $\|\nabla_u \hat{J}(u)\|_\infty$ also converges, confirming the success of the algorithm. Their plots are presented in Fig.12 and in Fig.13.

The graph in Fig.12 shows an initial rapid decrease, indicating quick battery charge improvement, followed by convergence to a stable -3.58 eV. This surpasses the highest energy state x_9 in experiments starting from $x_0 = 3$ (Table 2). Optimal control $u^*(t)$ allows surpassing energy limits of direct eigenstate transitions, guiding the system to a local minimum with higher energy than eigenstate x_9 of Hamiltonian $(\hat{H}_{mol} + \hat{H}_{hop}) \otimes \hat{I}_{cav}$. This highlights the algorithm's efficiency in maximizing energy storage by accessing otherwise unreachable states.

The optimal control trajectory $u^*(t)$, depicted in Fig.14, exhibits two significant peaks at the beginning, followed by damped oscillations, suggesting the need for intense initial application

and subsequent fine modulation for optimal charging.

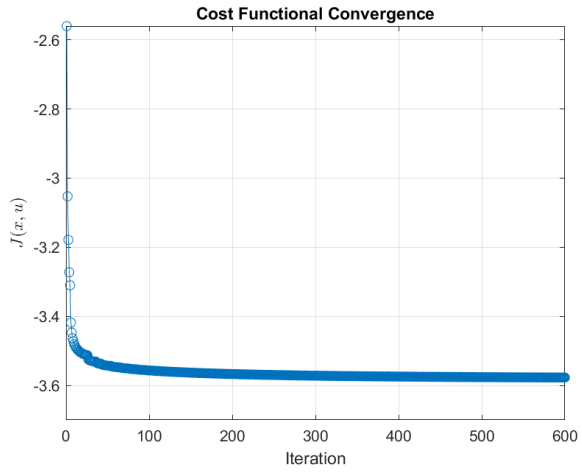

Figure 12: Convergence of the cost functional $J(x, u)$ during the optimization of battery charge.

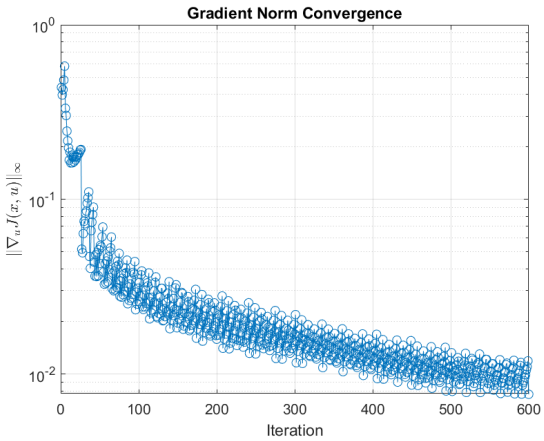

Figure 13: Convergence of the gradient norm $\|\nabla_u J(x, u)\|_\infty$ during the optimization of battery charge.

7. Conclusions and Research Perspectives

We showed that energy excitations in a quantum battery system are possible using a time-driving field for specific eigenstate transitions, indicating potential for optimal control to improve charging. However, large energy transitions remain challenging, even in small systems ($N_p = 2, M = 3$), raising doubts about the efficiency of the time-driving field. While our method can trigger energy transitions, it struggles with substantial energy transfers, particularly in larger systems. Our analysis uncovered key dynamics like intermolecular hopping, dissipation, and state connectivity, identifying stable conditions where control strategies work. These findings are crucial for reliable charging protocols. Although achieving practical application levels is difficult, our work advances the understanding of quantum batteries and sets the stage for future research, addressing current challenges.

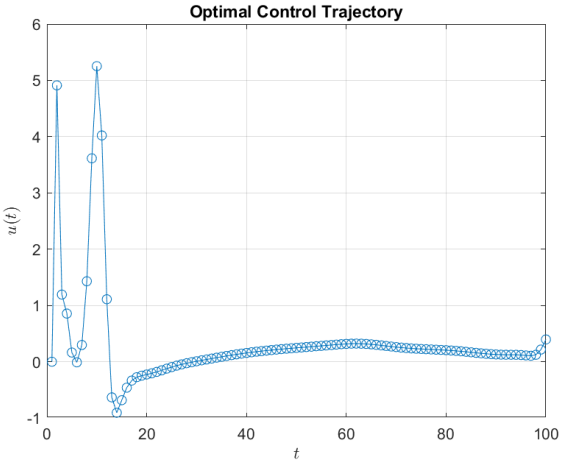

Figure 14: Optimal control trajectory $u^*(t)$ for maximizing battery charge.

This study proposes future research avenues. First, alternatives to the time-driving field approach, including different control fields, optimization algorithms, or hybrid classical-quantum strategies, could enhance quantum battery charging. Fourier decomposition of the control signals $u^*(t)$ may identify key frequencies for laser pulses. Using bias voltage V_b as a control parameter is promising due to its role in energy transfer within the Fermi-Dirac functions in Lindblad superoperators V_b. Optimal control strategies with multiple parameters $\eta(t)$, $V_b(t)$ could greatly improve charging, needing solutions for control problems with a number of controls $N_C > 1$, possibly time-dependent V_b. Second, improved computational methods and resources could simulate larger systems, exploring parameters for greater energy capacity. Finally, practical methods to convert quantum energy to electrical charge and prototype quantum battery devices are crucial.

References

[1] G. Ciaramella and A. Borzì. Skryn: A fast semismooth-krylov-newton method for controlling ising spin systems. *COMPUTER PHYSICS COMMUNICATIONS*, 190:11, 2015.

[2] G. Ciaramella, A. Borzì, G. Dirr, and D. Wachsmuth. Newton methods for the optimal control of closed quantum spin systems. *SIAM Journal on Scientific Computing*, 37(1):A319–A346, 2015.

[3] James Q. Quach, Kirsty E. McGhee, Lucia Ganzer, Dominic M. Rouse, Brendon W. Lovett, Erik M. Gauger, Jonathan Keeling, Giulio Cerullo, David G. Lidzey, and Tersilla Virgili. Superabsorption in an organic microcavity: Toward a quantum battery. *Science Advances*, 8(2):eabk3160, 2022.